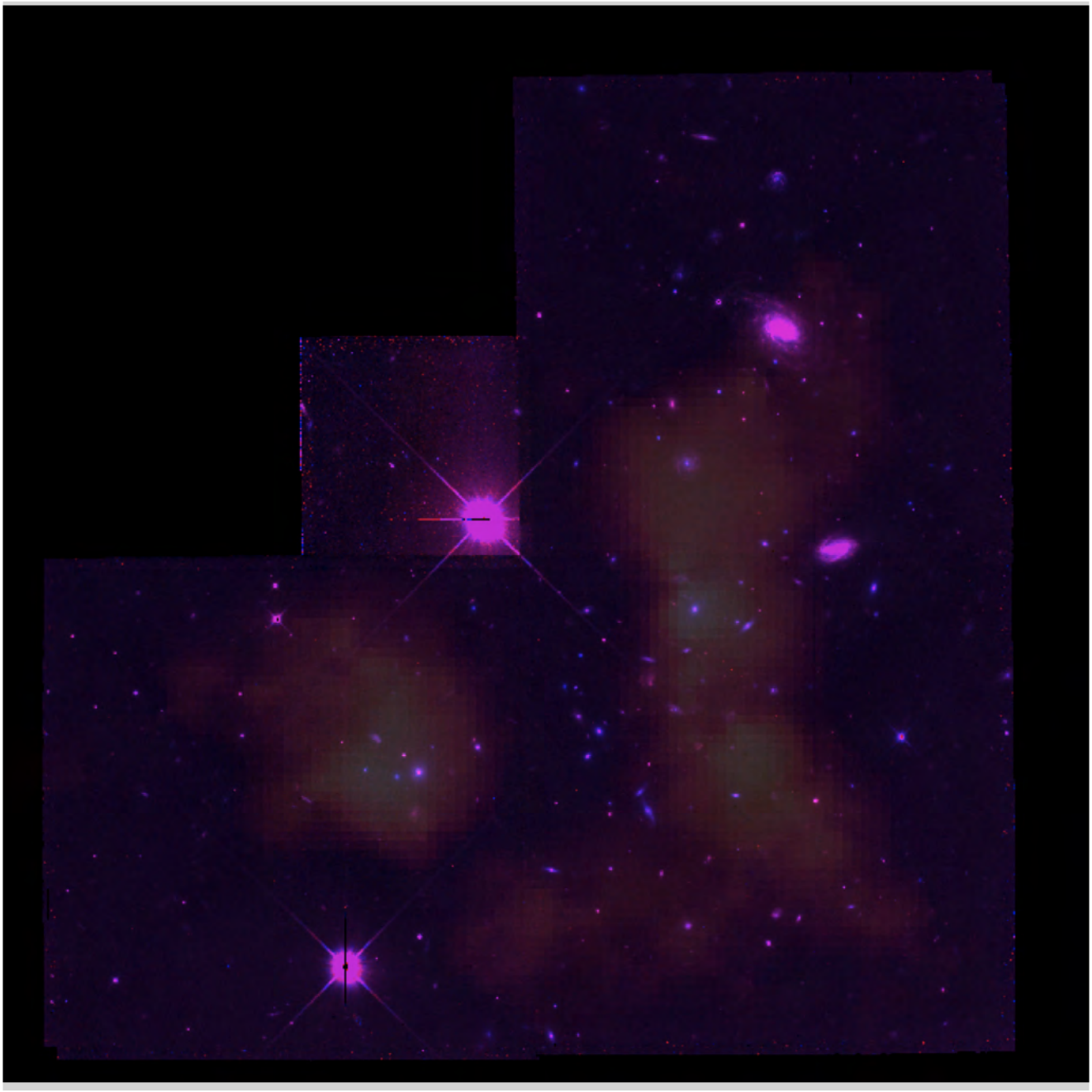

Searching for Self-Interacting Dark Matter Through Galaxy Cluster Collisions

Alex Moskowitz

April 2015

ABSTRACT

One proposed solution to the dark matter problem is a form of particle dark matter that only interacts (possibly strongly) with itself, so-called "Self-Interacting Dark Matter" (SIDM). SIDM has the potential to be tested with galaxy cluster collisions by looking for an offset between the SIDM and the galaxies of the cluster. I investigated a method of searching for this offset using the galaxy surface number density as a measure of a cluster's galaxy centroid; this method has the crucial advantage that it does not require redshift data and so can be carried out quickly on many clusters. Contrary to expectations, significant separations between the dark matter and the number density peaks are seen even in non-colliding clusters. The direct cause(s) of this offset remains unclear.

1: INTRODUCTION

1.1 The Dark Matter Problem

Dark Matter (DM) is an unsolved problem in astrophysics that has persisted for decades. In the 1930s, Fritz Zwicky measured the velocities of galaxies in the Coma galaxy cluster and found that the galaxies were moving too fast for the cluster's gravity to hold them in; apparently, there was more mass in the cluster than was visible. At the time, not much was known about galaxy clusters so the discrepancy was ignored. However, Vera Rubin noticed in the 1970's that galaxies contained a similar problem–given the mass that we can see in galaxies, their gravity should be so weak that their stars should simply fly out of them. It became apparent that some new type of matter, one that did not give off light, dominated the universe[1]. Further studies showed that DM rarely interacts with normal matter and accounts for 26% of the energy density of the universe[2]. DM is different than the "normal" baryonic matter that makes up galaxies, nebulae, stars, and planets; DM plays a significant role in particle physics and theoretical physics, pointing the way past the Standard Model.

A vast array of searches for DM have been conducted, but none have produced definitive results as to what DM actually is. These searches look for two important quantities: the mass of the DM particle, and its "cross-section," a measure of how well it interacts with matter. Finding the cross-section yields insight into what forces, other than gravity, DM participates in. DM detection can be separated into three types of experiments: production, direct detection, and indirect detection. In production, physicists attempt to create and study DM using particle accelerators such as the Large Hadron Collider at CERN. Direct searches try to find the DM particles that constantly pass through the earth. These experiments typically involve sensitive cryogenic detectors placed underground to shield them from cosmic rays. If a DM particle collides with a particle in the detector, it will generate light or sound that can be analyzed and compared to the signal from known particles. However, direct detection experiments have yet to find a conclusive result. Direct detection also faces drawbacks. It is possible (albeit unlikely) that the solar system exists in a part of the Milky Way that lacks dark matter, which would render all direct detection experiments useless.

The third method of DM search is indirect detection. These experiments look for the collision of DM particles with either normal matter or other DM particles, or the decay of DM particles. These processes could produce gamma rays, antiprotons, or positron cosmic rays. While these searches occasionally yield a tantalizing signal (such as the excess positrons observed by the PAMELA detector[3]), no conclusive proof exists for a DM candidate. This is due to a few problems with indirect detection. Like direct searches, we can only use the Milky Way (and possibly a few nearby galaxies) to look for gamma rays; because cosmic rays change direction and energy in the galactic magnetic field, determining their source is difficult. Most importantly, any DM signal in these modalities has a high and poorly understood background.

DM can also be studied through weak gravitational lensing. General Relativity posits that matter bends space. Therefore, a massive object such as a galaxy cluster will bend the light that travels near it. In particular, an image of a galaxy will get stretched and sheared, changing its ellipticity (defined as $\frac{a^2-b^2}{a^2+b^2}$, where a and b are the major and minor axes of the galaxy's image, respectively). Weak gravitational lensing exploits the fact that these ellipticities are usually randomly scattered on the sky. Gravitational lensing distorts the ellipticities in a predictable way and so by measuring the distribution of elliptitcies above random, one can reconstruct the mass required to bend space in that manner. This is famously demonstrated in the Bullet Cluster. One theory of DM held that physicists simply had mechanics wrong, instead of explaining the rapid rotation of galaxies by a new form of matter; $F = ma$ might not hold for low accelerations, allowing stars that orbited on the outskirts of galaxies to move at a high velocity without flying out of the galaxy. The Bullet Cluster, which was actually two galaxy clusters that had previously collided, provided a definitive test of this. Galaxy clusters are made up of galaxies, hot gas, and DM. Most of the normal "baryonic" mass is in the hot gas. When the clusters collide, the galaxies and DM pass through each other because the galaxies are mostly empty space, and DM is assumed to not interact with itself. However, the gas of each cluster does collide, forming a shock wave and decelerating. If there is no DM, the gravitational lensing peak should be with the decelerated shocked gas, because that is where most of the baryonic matter is. If there is DM, the gravitational lensing peak should lie with the galaxies, because the DM makes up most of the mass of the cluster and can pass through the other cluster relatively undisturbed. The Bullet Cluster conclusively showed that the lensing peak lay with the galaxies, confirming the DM theory. It is extraordinarily difficult to replicate this result with a modified dynamics theory.

2.1 Self-Interacting Dark Matter

A new search method is possible if the dark matter takes the form of SIDM. The method involves two galaxies clusters that have collided. As described above, the gas shocks and experiences drag, and the DM and galaxies pass through each other. However, if the DM interacts with itself, it will also experience a drag force, with fluid-like properties. This drag force will slightly separate the SIDM from the galaxies in the cluster. By comparing the centroid of the galaxies and

Figure 1: An image of the Bullet Cluster, along with hot gas (pink) and matter inferred from gravitational lensing (blue). The two are clearly separated.[4]

the centroid of the SIDM (found through weak lensing), constraints on the property of SIDM can be found. The optical depth τ of the DM in the cluster is given by $\tau = \Sigma\frac{\sigma}{m}$, where Σ is the DM surface density, σ is the SIDM cross-section, and m is the mass of the SIDM particle. By requiring $\tau < 1$ (or else the clusters would not have passed through each other), a constraint on $\frac{\sigma}{m}$ can be found when Σ is computed via weak lensing[5]. The SIDM-galaxy offset could also occur in individual galaxies falling into a dark matter halo, as the recent claim of Massey *et al.* demonstrates, although this possibility is not discussed here.

Searches for SIDM have several advantages over other DM searches. First, SIDM is model independent, which gives it the ability to discover new dark sector forces[6]. SIDM searches can be carried out with existing telescopes. This is particularly important because it could provide confirmation to a detection in another modality without developing a specialized detector just to do so. Although colliding clusters are rare, they are numerous enough that many of them will be found in the future. Finally, SIDM, if real, would play an important role in cosmology. Obviously, cosmological studies of cluster collisions would have to take this into effect[1]. However, SIDM can solve other problems as well, such as the core-cusp problem in galaxies[5].

While the separation between the gas and the galaxies of colliding clusters is easily explainable by a drag force, the situation is more complicated with SIDM because the galaxies are gravitationally bound to the DM. Two types of SIDM interactions are possible: "frequent, low momentum transfer" and "infrequent, large momentum transfer" scenarios[6]. These mechanism change the DM location through different methods. In the frequent interaction scenario, some of the DM evaporates, which yields a drag force dependent on σ. In the infrequent scenario, the scattering angle is directly opposed to the cluster motion, and so the redirected DM skews the distribution backwards. The fraction of particle interactions that result in the evaporation of the particle is designated as f; $f < 1$ must be true, because no colliding clusters are observed without their DM halo. For example, the Bullet Cluster gives and estimate of $f \approx .6$. In the infrequent, large momentum transfer scenario, a better constraint on $\frac{\sigma}{m}$ is given by

$$\Delta M_{cluster} = \frac{\Sigma f \sigma}{m}$$

where $\Delta M_{cluster}$ is the mass that the cluster loses in the collision.

When calculating the center of the DM, the peak of the DM, and not the centroid, should be used. Particles ejected during the collision move away from the clusters, skewing the centroid in their direction. Because of tidal forces, DM near the edge of the halo could escape independent of any interaction. Furthermore, they would no longer be considered part of the cluster. Fortunately, because the lensing signal depends on column density, they do not contribute greatly to the lensing analysis. DM that evaporates from the smaller of the two clusters is still bound to the larger, and this increases the lensing signal of the larger cluster. By subtracting the background of the lensing distribution, these two effects make it possible to distinguish between the large and small momentum transfer scenarios.

Another effect to consider is the gravitational interaction between two DM particles. Because gravity is weaker than other possible interaction forces, all of the direct gravitational interactions would fall under the frequent, small momentum transfer scenario. In this case, the typical disturbance Δv to a particle's velocity v is given by

$$\frac{\Delta v^2}{v^2} = \frac{8 log N}{N}$$

where N in the number of particles in the cluster, at least 10^{60}. This makes the effect small, so the direct gravitational interactions between particles can be ignored and the cluster potential can be assumed to be smooth.

In the reference frame of the galaxies, they feel an acceleration relative to the DM. A constant acceleration will add a linear potential to the DM gravitational potential. Moving in this new potential, some of the galaxies exceed the escape velocity of the cluster and begin to leave. This biases the galaxy centroid in their direction. While galaxies near the center of the cluster may also feel an acceleration relative to the SIDM, they are more strongly bound to the cluster's DM, and thus the separation is smaller for them.[6]

Several assumptions have to be checked in order for this analysis to succeed. It is possible for an object in the foreground to cause a second lensing peak and falsely indicate the colliding cluster; this can be checked by looking for shocked gas, or by redshift analysis. Secondly, the lensing signal could be caused by two line of sight DM filaments. Most of the time, unlikely; for example, with the Bullet Cluster, the probability that this would happen is approximately 10^{-11}.[7] However, checking this would require redshift data, which were not available for all of the used clusters.

Several different "centroids" exist for a galaxy cluster, and they all yield a measure of the separation between the SIDM and the galaxies of a cluster. One canonical way of defining the centroid of a galaxy cluster is through its brightest galaxy. However, because a sources of separation are the evaporating galaxies (or at least the galaxies not directly in the center of the cluster), this is not a good measure. The next obvious choice is the geometrical centroid of all of the galaxies is the cluster. This has several disadvantages, however. First, if the

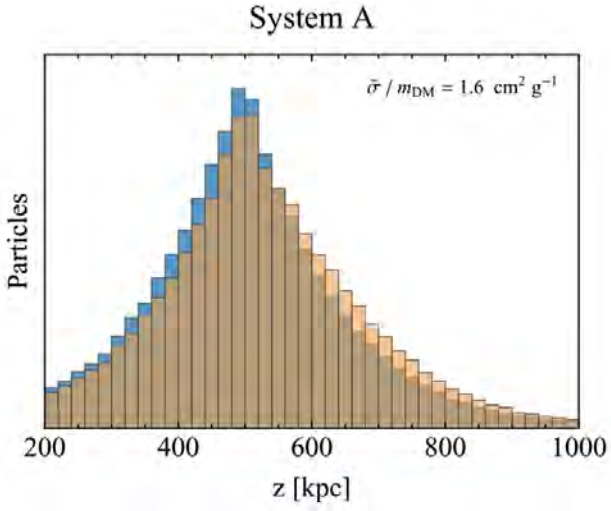

Figure 2: The distribution of galaxies (tan) relative to the DM (blue) and overall cluster (brown) from a simulation of a typical galaxy cluster collision.[6]

image itself is oddly shaped–as is the case with the Hubble WFPC2 images–the centroid is biased towards the centroid of the image itself. Secondly, in order to remove background galaxies (which also causes the cluster centroid to be biased in the direction of the image centroid), redshifts (or at least multiple accurate colors) must be computed. This requires additional telescope time.

Instead, I use the peak of the galaxy number density as the measure of the centroid. This is accomplished by assigning each pixel in the image a value equal to the number of galaxies in a given radius R around it. This solves problems that arise with the geometric definition of the centroid. Because the center is not computed from a global distribution of objects, the effect of image geometry is negated. While all of the background galaxies contribute to the geometrical centroid if they are not removed, the cluster galaxies overwhelm the field galaxies near the center of the cluster. A second effect of this overwhelming by the cluster galaxies is that the analysis can be performed with only one filter. This provides a quick way to reject candidates without wasting valuable telescope time taking redshifts. Because so few cluster collisions are known, the ability to identify many candidates is a major advantage. For SIDM colliding clusters, one would expect any offset to be on average along the line of collision, but there are currently too few known cases to test this.

One possible problem with this method could be that if R is too small, it won't include the higher-offset galaxies near the edge of the cluster. However, this does not cause a significant problem. Figure 2 shows that even near the center of a cluster, there is still an excess number of galaxies than expected compared to the dark matter. A demonstration of this fact is given in Figure 3. The theory of Kahlhoefer *et al.* (henceforth referred to as F14) predicts that as you include galaxies farther away from the cluster center in the number density calculation, the offset should increase; Figure 4, using the one-dimensional simulations of F14 as source data, confirms this effect.

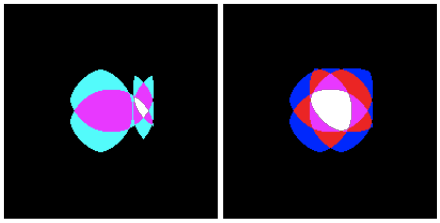

Figure 3: Left: Number density derived from a symmetric test cluster made from a handful of galaxies arranged symmetrically. Right: the same test cluster, but with some of the outskirt galaxies shifted to the right. The peak is the white area; it is apparent that the peak does shift if the outskirt galaxies are shifted. As the number density of galaxies grows, the peak location also becomes smaller, so the wide peak area of the left image is simply a reflection of the low number of objects used to create the test cluster.

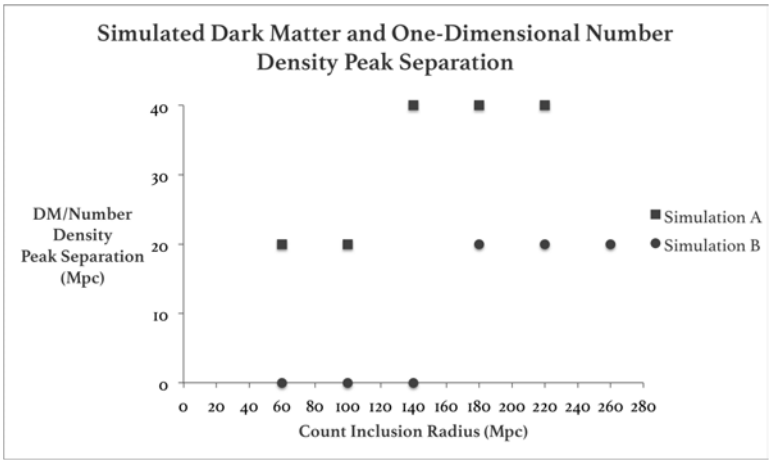

Figure 4: Dark matter and number count density peak separations taken from the 1-dimensional simulations of F14. The horizontal axis is the radius inside which objects were included in the number density calculation. The offset is small but nonzero for sufficiently large count inclusion radii.

2: METHODOLOGY

2.1 Software

The following existing software was used in the analysis:

- Source Extractor (SE), software that analyzes astronomical images and extracts objects (stars, galaxies) as well as information about those objects such as location, size, and brightness.
- Fiatmap, software that takes a catalog of galaxy locations and geometrical moments and computes a weak lensing calculation using it. The software returns an image showing the location and relative amount of mass that give the ellipticity deviations above random that were present in the catalog.
- Sex2fiat, software that converts an SE-formatted catalog into a fiatmap-formatted catalog

• IRAF, an astronomical image processing software package that contains a multitude of functions used in astronomical analysis. In this project, IRAF was used to align several images of the same cluster.

• DS9, software that lets the user view FITS images. In addition to viewing images, the software also lets the user create shapes at specified coordinates, which was useful for noise and foreground star elimination.

• Microsoft Excel and Microsoft Powerpoint

• Python, Anaconda distribution, which includes various scientific packages.

• Fitsio, a package for Python that enables FITS reading and writing.

• PyFits, a package for Python that enables FITS reading and writing.

In addition to this, I created a python module designated "se_tools". se_tools contains the following functions:

• *sefile_to_xyvalue*, which takes a catalog in SE file format and turns it into a python list

• *find_centroid*, which finds the (possibly weighted) centroid of a list of objects

• *se_centroid_noweight*, which finds the unweighted centroid of a list of object

• *se_randomcat*, which takes a catalog and creates a new catalog with a specified fraction of objects taken at random from the original catalog.

• *se_randomcat_corner*, which performs that same actions as *se_randomcat* but adds a small object at each corner of the image that the catalog was taken from

• *keep_within_r*, which removes all objects a given distance away from a given point in a catalog

• *centroid_stats*, which generates a given number of random catalogs from a given catalog and computes the centroid of each of them

• *ds9_box_rmvpoints*, which removes objects from a catalog if they are inside a given box, in the format of DS9's "box" object. This way, one can easily draw boxes around objects in DS9 and then remove them

• *value_cut_gt* and *value_cut_lt*, which remove objects from a catalog if a their value in a given column in the catalog is greater than or less than a certain value

• *align_assoc*, which combines catalogs from two images of the same cluster that have been generated using SE's ASSOC function (which identifies the same objects in the two images)

• *sex2bpz3*, a function which takes 3 catalogs in SE format and converts them into the format of BPZ, a piece of software that computes photometric redshifts

• *sex2bpz2*, which acts like *sex2bpz3* but works with two catalogs instead of three

• *sex2bpz2_wfpc3*, which acts like *sex2bpz3* but computes magnitudes for images taken with the Hubble WFC3

• *sex2bpz3_wfc*, which acts like *sex2bpz3* but computes magnitudes for images taken with the Hubble WFPC

• *sex2bpz3_wfc_f*, which acts like *sex2bpz3* but computes fluxes for images taken with the Hubble WFPC. After extensive testing, it was determined that BPZ requires more than two images to give accurate results, and so was not used for further analysis

• *scale_catalog*, which takes a catalog and scales the location of all of its objects by given factor

• *check_for_duplicates*, which checks if a column in a catalog has duplicate entries

• *gauss*, which adds a gaussian function near each catalog object's position to a blank FITS image

• *bigger_rad_gauss*, which acts like *gauss* but with a variable dispersion for the gaussian function

• *weighted_gauss*, which acts like *gauss* but has the ability to be weighted by a column in the catalog

• *exp_image*, which acts like *gauss* but uses an exponential instead of gaussian function

• *sersicn_image*, which acts like *gauss* but uses a sersic profile ($e^{\frac{-\alpha r}{n}}$, where α is a constant and n is an integer) instead of a gaussian function[8]

• *count_points*, which assigns to each pixel in an image the number of objects within a given radius of that pixel. To reduce run time by skipping pixels with zero value, the algorithm actually goes through the catalog of objects and adds 1 to any pixel within a given radius of that object. The image size can be scaled down by a given factor to increase run speed.

• *color_cut*, which removes objects from a catalog whose color (defined as the ratio of fluxes in two separate images) does not lie between given values

• *get_peak*, which find the greatest value of a FITS image

• *get_peak_search*, which finds the greatest value within a certain radius of a given point in a FITS image

• *get_peak_centroid*, which finds the geometric centroid of all the peak values within a certain radius of a given point in a FITS image

• *random_count_stats*, which first creates a number of random catalogs using *randomcat*, then creates number density images from those catalogs with *count_points*, and finally extracts the peak of the image with *get_peak_centroid*

• *fiatrand*, which uses *randomcat* to generate random catalogs and then creates a script to run sex2fiat and fiatmap on those catalogs

• *SE_stats*, which analyzes fiatmap images created using *fiatrand*. It searches for lensing peaks within a given radius of given coordinates in the image by running SE on the fiatmap images

• *calc_distance*, which calculates the distance between each object in a catalog and a given coordinate

• *circle_filled_fraction*, which calculates how many nonzero pixels in a specified FITS image are in a given circle

The functional part of se_tools is roughly 1700 lines long. Including test cases and scripts to run se_tools on each cluster, the total amount of code is more than 3000 lines.

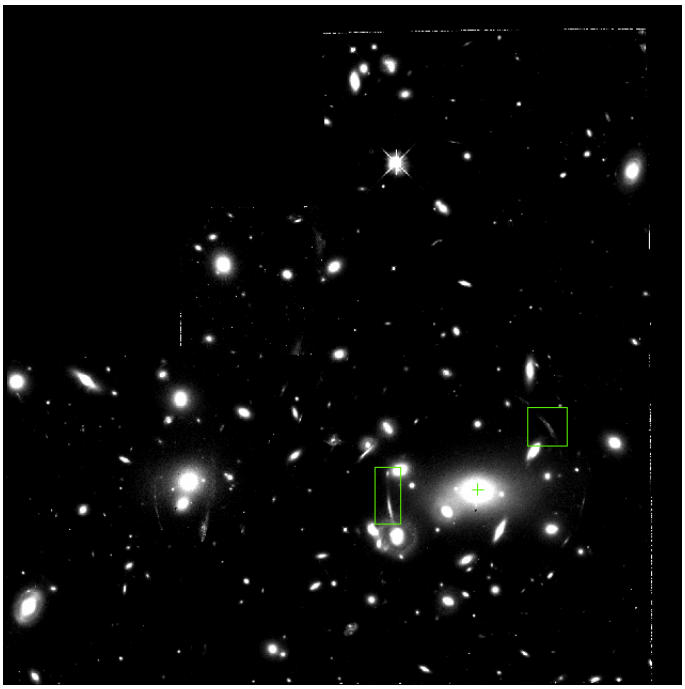

Figure 5: An example of a cluster (A2218) that is easily identifiable as one; note the bright central elliptical galaxies (+) and strongly lensed galaxies (boxes).

2.2 Cluster Identification

Cluster candidates were taken from the Hubble Space Telescope image archive. In the interest of time (so as to not redetermine analysis parameters) only those taken with the Hubble Wide Field Planetary Camera 2 (WFPC2) were used. Some clusters were easily identifiable; one is shown in Figure 5. Candidates that were less obvious were first sorted by image quality (absence of artifacts) and number of objects (as will be shown below, too few objects causes problems in the lensing mass reconstruction). For those images that met these criteria, a lensing analysis and number density were both calculated. Those images that contained both a clear lensing peak and a clear number density peak were kept. The features did not necessarily have to align with each other or a clear feature of the cluster (such as a bright elliptical) because the sough-after effect is a separation between these features. The clusters that were selected for analysis are listed in Table 1.

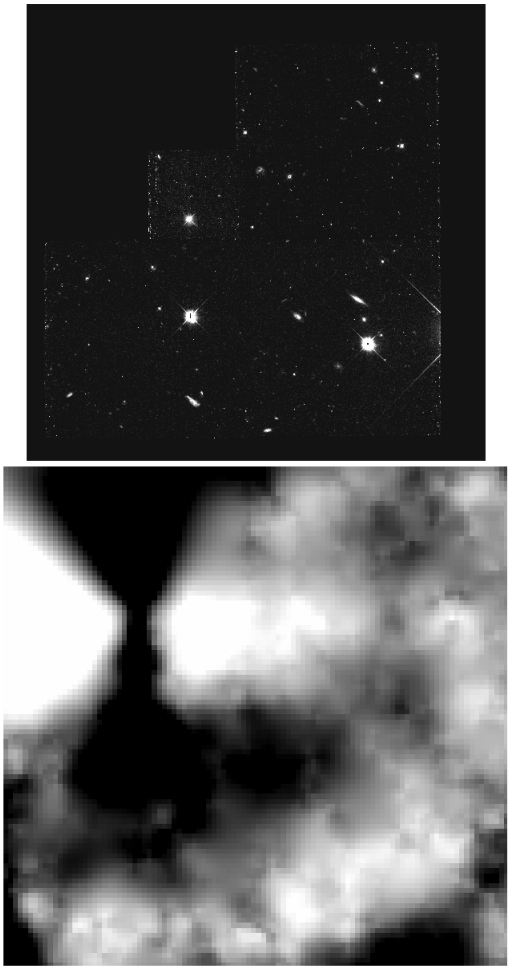

Figure 6: Top, a candidate image (f08219+0331). Bottom, a lensing map of that image. This image is rejected due to lack of a clear lensing peak; the apparent peak on the left side is an artifact of the bright white line at the left side of the Planetary Camera CCD in the Hubble image and would be removed during the lensing analysis phase.

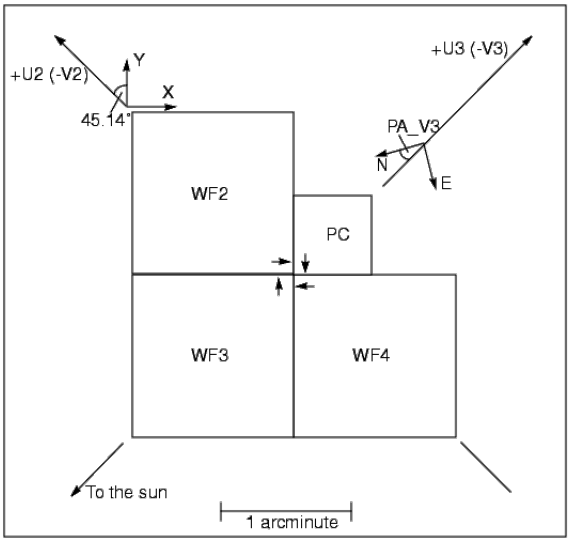

Figure 7: A diagram of the Hubble Wide Field Planetary Camera 2 detector showing the locations of the Wide Field CCDs (WF) and the Planetary Camera (PC). The V3 vector depends on the target location. This diagram is facing the detector, so the images themselves are mirrored.[9]

Name	RA	DEC	Filter(s)
CL1322+302	201.206	30.9750	F606W, F814W
CL0016	4.64017	16.42942	F814W, F555W
CL0024	6.64843	17.1619	F814W, F450W
CL0054	14.2274	-27.6753	F814W, F555W
CL2244	341.803	-0.2.09438	F814W, F555W
CL1446	222.367	26.1323	F702W
CL1322+311	201.206	30.1892	F606W, F814W
CL1603	241.076	43.0767	F814W
5C210	163.147	48.6683	F814W, F555W
MG1131	172.985	4.93061	F814W, F675W
CL1601	240.793	42.7597	F702W
A2218	248.987	66.2105	F702W
MS1054	164.248	-3.62449	F814W
CL0412-6550	63.2152	-65.8381	F184W

Table 1: Clusters used in this project. If two filters were present, lensing analysis was carried out on the first image listed.

2.3 Catalog Cleaning and Random Catalog Creation

SE works by finding high contrast clusters of pixels. Therefore, objects along the edge of the data portion of the image must be removed. This is fairly easy; boxes can be drawn around the edges of the image in ds9, and then their coordinates are exported into *ds9_box_rmvpoints*. Improper edge removal contaminates both the lensing reconstruction and the galaxy density. The edge artifacts on the left hand side of the WFPC2 lie along right angles, which fiatmap interprets as a massive object in the upper left hand corner of the image. This effect in demonstrated in Figure 6. In the number density image, the edge artifacts vastly outnumber the galaxies

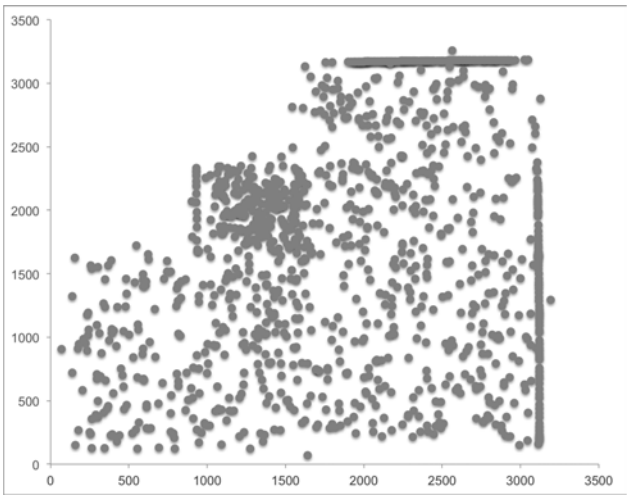

Figure 8: A plot of object pixel locations in a WFPC2 image without artifact and PC CCD removal, clearly showing the large number of these objects in the affected areas.

near them and so they form the number density peak of the image. For similar reasons, the PC CCD is cut from the images unless the cluster center lies in it, as it is significantly noisier than the WF CCDs and so its number density is artificially inflated under optimal SE noise settings for the WF CCDs.

While some stars are removed, they do not significantly hurt the quality of the results. Bright stars are obvious due to their X-shaped spikes. As Figure 9 demonstrates, even without the presence of a cluster, faint stars make up such a small fraction of the objects that they should not significantly change any of the results.

Some of the clusters had images taken in two different filters. Most multiple-filter cluster images were already aligned, but those that were not were aligned using IRAF. For these clusters, a rough "color" of each galaxy was calculated, defined as the ratio of fluxes in two different filters. Elliptical galaxies have a different color than spiral galaxies or galaxies not in the cluster, which provides a way to isolate cluster galaxies. To do this, ten bright ellipticals in the cluster were identified, and only those galaxies whose colors were within several (usually two or three) standard deviations of that color were used. The number of standard deviations varied because the colors were sometimes close to 0 and using three standard deviations would make the lower limit negative, which would keep all unwanted galaxies that had very small colors.

The ten "sample" ellipticals had to be identified by hand. Ellipticals differ from spirals in that their cores are very bright, but their light falls off quickly as one moves away from the core. By comparing the image with a bright value cutoff and then a dim value cutoff, it is possible to distinguish between spirals and ellipticals, as is demonstrated in Figure 10.

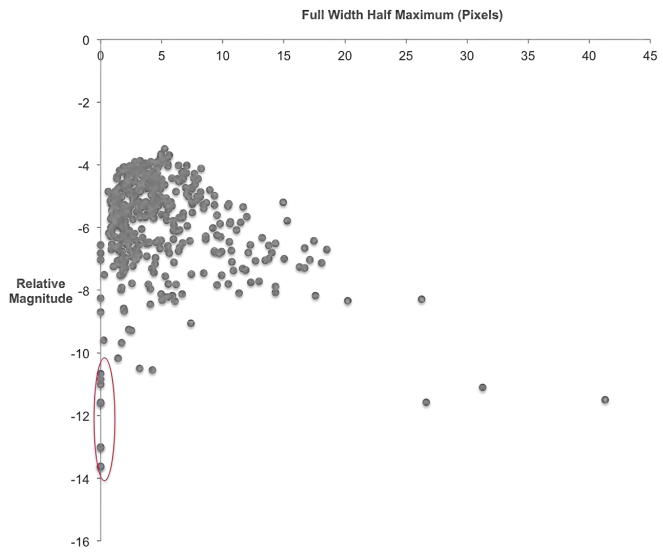

Figure 9: A plot of object Full Width Half Maximum, in pixels, versus non-normalized magnitude for the non-cluster target f06512+7917. Possible faint star objects, which are much brighter than their size would predict, lie within the red oval.

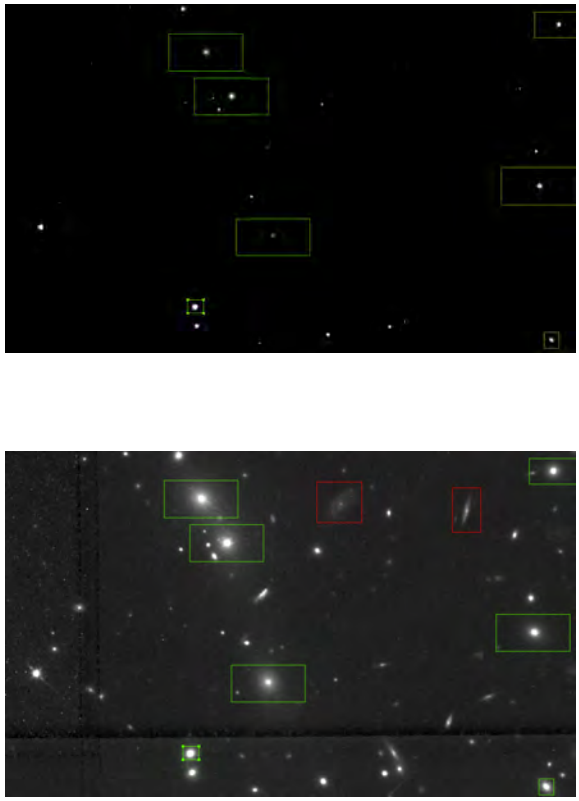

Figure 10: Top: an image of galaxies with a high brightness cutoff. Bottom: The same image with a low brightness cutoff. While the cores but not the outskirts of ellipticals (green) are visible in the high cutoff image, the entire core and disk of a spiral (red) show up when the cutoff is lowered.

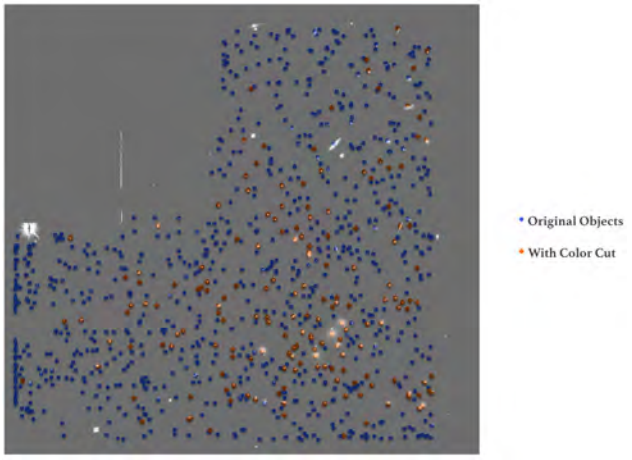

Figure 11: A plot of object position for CL0024, with objects before (blue) and after (orange) the color cut. The increase in the number density of color-cut objects approaching the cluster center is clearly visible.

Name	$\frac{\sigma_{color}}{mean_{color}}$
CL1322+302	0.58
CL0016	0.29
CL0024	0.13
CL0054	0.15
CL2244	0.077
CL1322+311	0.71
5C210	0.15
CL0739	0.54
MG1131	0.51

Table 2: Ratio of standard deviation of color values divided by the mean color value for multiple-filter clusters. In all cases, the standard deviation is less than the mean, indicating that the galaxies selected to use as a basis for the color cut were likely part of the cluster.

For both the number density and lensing maps, 30 random catalogs were used in order to calculate uncertainties. For the number density maps, each random catalog contained 75% of the catalog (color-cut when available). For the lensing map, the color cut was not applied, and 75% of the objects in the full catalog were used. If too few objects are used in the lensing reconstruction, quadrupole noise develops (see Figure 12), which is why 75% was chosen. Because weak lensing measures alignment above random noise, the presence of objects not in the cluster does not significantly skew the results. For the lensing catalogs, small test objects with locations at each corner of the image were added to the end of each catalog. If this is not done, the fiatmap image is not square and there is also nothing to align it to in the original image. This means that mapping fiatmap image coordinates to original image coordinates is impossible. Adding corner objects forces the image to be square and forces its corners to match those of the original image. After creating the images, source extractor is used to extract the lensing peak. In the case of multiple peaks, the nearest peak to the full catalog peak in each randomized trial was kept for analysis. Although this could potentially contribute a bias, this does not appear to be the case, as Figure 20 demonstrates.

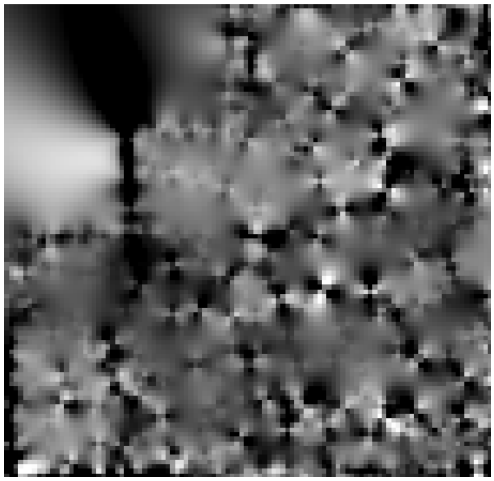

Figure 12: An example of the quadrupole noise created by fiatmap if the number of objects is too low, or the parameters are set incorrectly.

2.4 Selection of Centroid Measure

Because the geometric centroid is too easily influenced by the image geometry, a new way of defining the "centroid" of the cluster is needed. Several possible ways of defining a centroid exist. One possible method is to start with an empty image. For each object, the value of a specified function is added to the pixels around its location. This function is proportional to an object's flux, and its width is a function of the object's radius. Ideally, the centroid of the cluster would be the peak of this image, because many objects' functions would overlap with near the center of the cluster. Gaussian, exponential, and sersic (with n=4) functions were tried. As can be seen in Figure 13, while each map contains significant aesthetic value, none of them provide a unique definition of the centroid of the cluster. The unweighted gaussian and exponential functions fall off too fast, and so no significant overlap is achieved. The weighted gaussian and exponential functions, as well as both sersic profiles, are too easily influenced by bright galaxies, which is a particular problem because field galaxies may be brighter than most cluster galaxies.

Instead, a "number density" map was used. The value at each pixel is the number of objects within a given radius, usually a few hundred pixels, henceforth known as the "inclusion radius". This method gives an easily identifiable peak that is not influenced by the presence of any single galaxy. The peak value of this map is used as the centroid. Because the peak value usually exists at more than one pixel, the centroid of all points with a value equal to the peak value is used. The centroid maps were generated scaled down by a factor of 2 or 4 to increase computation speed; as this reduction factor is less than the reduction factor for the fiatmap images (by about a factor of 5), it is unlikely to significantly affect the results.

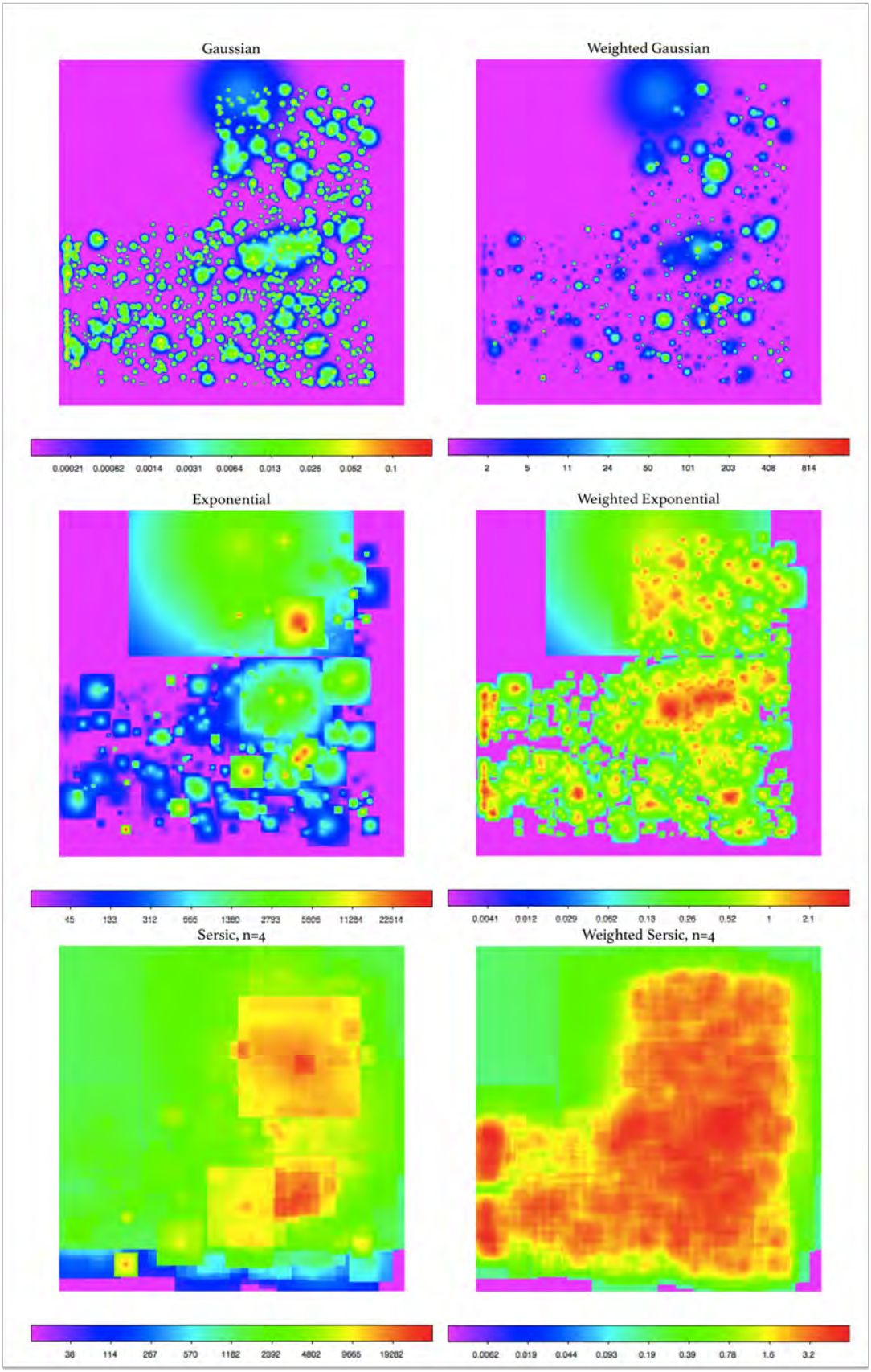

Figure 13: Several maps representing a different function at each galaxy position in the cluster CL0024. Values are arbitrarily normalized. The "square" effect is due to a low value cutoff implemented to reduce computation time.

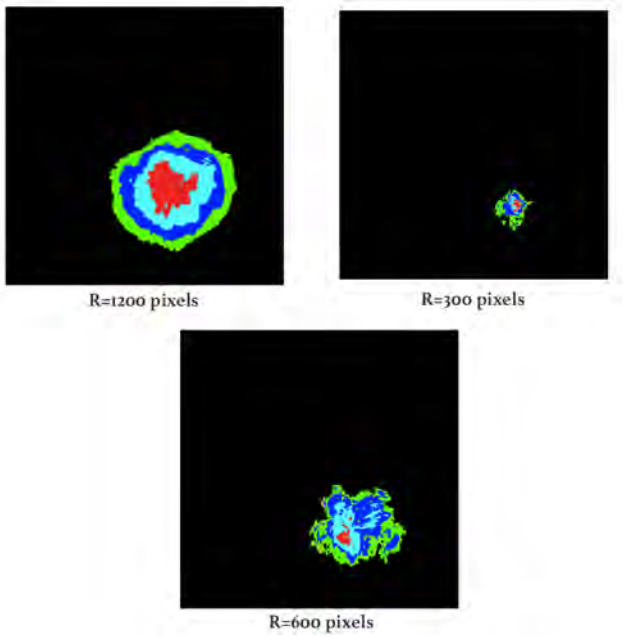

Figure 14: Number density contour maps for the cluster CL0024 for three different inclusion radii. Compared to those of Figure 13, the peak is singular, well defined, and there are no features due to individual galaxies.

3: RESULTS AND DISCUSSION

3.1 Results

The minimum offset is determined by dividing the pixel distance between the average position of the lensing and number density peaks by the standard deviation of the lensing peak or the number density peak, whichever is larger. The minimum distance is used because the requirement for separation is *at least* a one standard deviation difference between the peaks.

The offset pixel distance is converted to a relative physical distance by dividing by the full width half maximum of the number density count map; this FWHM remained stable for the two high values of inclusion radius and so the middle value was used. The FWHM normalization works on the principle that more distant clusters appear more concentrated in the sky. While cluster concentration is not a perfect adjustment method (because cluster concentration varies with cluster mass and redshift), it theoretically provides a more realistic indicator of number density inclusion radius. Surprisingly, as Table 3 and Figure 15 clearly show, there are significant separations even for clusters with only a single lensing peak.

Given the inherent nonmonotonic scatter observed in Figure 16 and in the other clusters, a more realistic measure of the minimum separation is found taking each separation d_i (where i is the particular inclusion radius) and computing an "adjusted separation"*

$$s_i = \frac{d_i}{standard\ deviation(d_i)}$$

While this estimate is more accurate, it blows up for small standard deviations, as is the case for CL1601. The adjusted results remain largely unchaged, with offsets even for single lensing peak clusters.

3.2 Possible Sources of Observed Separation

A possible bias could be due to eliminating many galaxies in the color cuts. However, as Figure 21 shows, there is no clear difference between those clusters with color cuts and those without. A third possible bias is the inclusion of the PC CCD for clusters where many of the objects fall into this CCD. Because of the high noise compared to the other CCDs, fake objects are often picked up, which would bias the number density count around the PC. As Figure 2 shows, the adjusted separations are in fact on average higher for those images that included the PC. This effect is statistically significant with a z-score of 2.6. However, this only explains part of the variation, as some separations without the PC are above 1 standard deviation.

Another possible explanation for the offsets is the inherent scatter in the number count position due to the nature of the random catalogs. Scatter in the peak position will, on average, increases (or at least on average does not decrease) the separation between the peaks, as Figure 18 demonstrates. The variation compared to the peak value is larger for lower inclusion radii, and the unadjusted scatter in separations is greater for lower inclusion radii (see Figure 15). However, Figure 19 demonstrates that this possible correlation does not hold on a case-by-case basis. The inherent scatter in the lensing position does not play a role because it is what was used to define the distance between the two peaks in the first place. It is, however, possible that the average of the lensing peaks generated by the random catalog is offset from the true position of the peak. To test for this, the difference between the average random peak and the full-catalog peak was calculated. As Figure 20 shows, however, this is not correlated with offset size.

One possible flaw is if the inclusion radii are not large enough to properly gauge any offset. While this may be the case for some of the images–comparing to the simulations in F14, the offset becomes visible in under one FWHM in simulation A but not in simulation B–it is irrelevant as significant offsets are seen even in those images without multiple lensing peaks. However, this does suggest that a telescope with a wider field of view than the Hubble Space Telescope would be better suited to this analysis. Ideally Hubble would be used to get the lensing peak (which depends more on high-resolution imaging of galaxies near the center of the cluster) and a wider field of view telescope should be used to calculate the number density; the resolution can be quite poor on the number density images and still give accurate results, as all that is needed is the position of the object. Another possible flaw is that the color cuts select for elliptical galaxies, which preferentially eliminate galaxies at the edge of the cluster. This effect would likely decrease any separation, as the galaxies not in the very center of the cluster are those that more strongly shift the number density away from the DM[6]. However, this does not offer an explanation of the excess observed separation.

*It has been suggested by Ian Dell'Antonio that a better correction would involve dividing by the quadrature sum of the errors. I have left it as stated partially because this represents a correction for variation regardless of the variation's cause, which remains mysterious, but mostly because I currently do not have the time to redo the analysis.

Cluster	Radius 1	Radius 2	Radius 3
CL1322+302 Multiple Peaks	3.2	3.4	1.6
CL0016 Single Peak	0.8	2.8	2.1
CL0024 Multiple Peaks	1.1	0.3	2.3
CL0054 Multiple Peaks	2.3	0.8	2.8
CL2244 Single Peak	0.2	2.2	1.7
CL1446 Single Peak	0.4	0.4	2.1
CL1601 Multiple Peaks	56.6	58.0	56.0
CL1322+311 Single Peak	9.9	8.0	8.3
CL1603 Multiple Peaks	2.2	0.20	1.1
5C210 Multiple Peaks	7.1	8.9	8.5
MG1131 Multiple Peaks	4.3	2.7	2.4
A2218 Single Peak	0.6	2.0	0.1
MS1054 Multiple Peaks	1.9	1.5	3.4
CL0412 Multiple Peaks	5.3	7.1	5.5

Table 3: Minimum number of standard deviations between dark matter and number count density peaks for each cluster, for three different object inclusion radii. Whether or not the cluster has multiple peaks in its lensing image is also indicated. Data has been adjusted for the inherent scatter in separation due to variation in the number density inclusion radius.

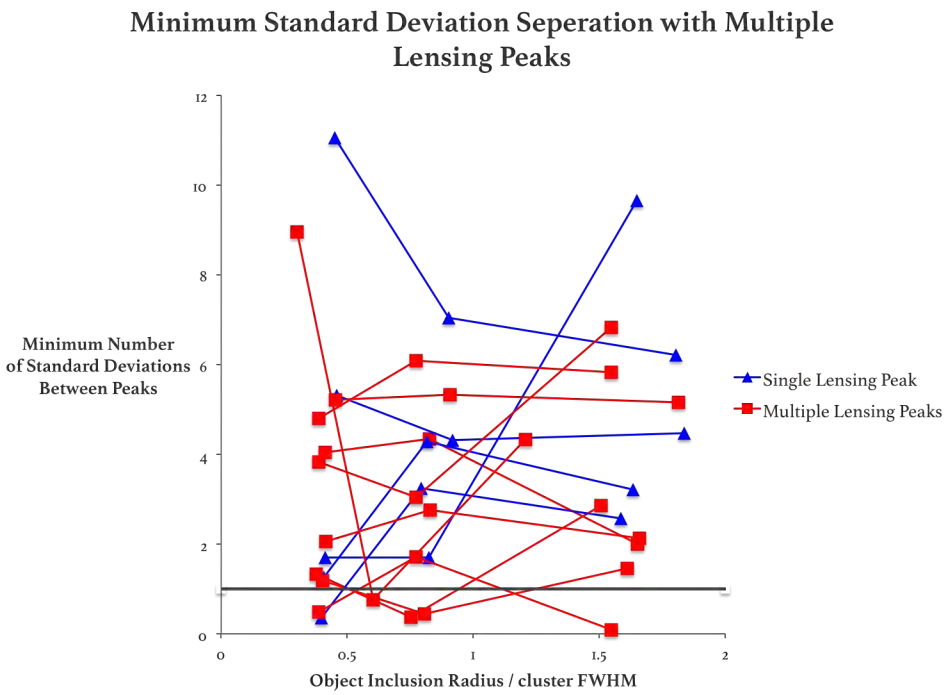

Figure 15: Minimum number of standard deviations between dark matter and number count density peaks for each cluster, unadjusted for inherent scatter. The gray line demarcates a one standard deviation difference. There is no clear difference between images with multiple lensing peaks and those with only one peak.

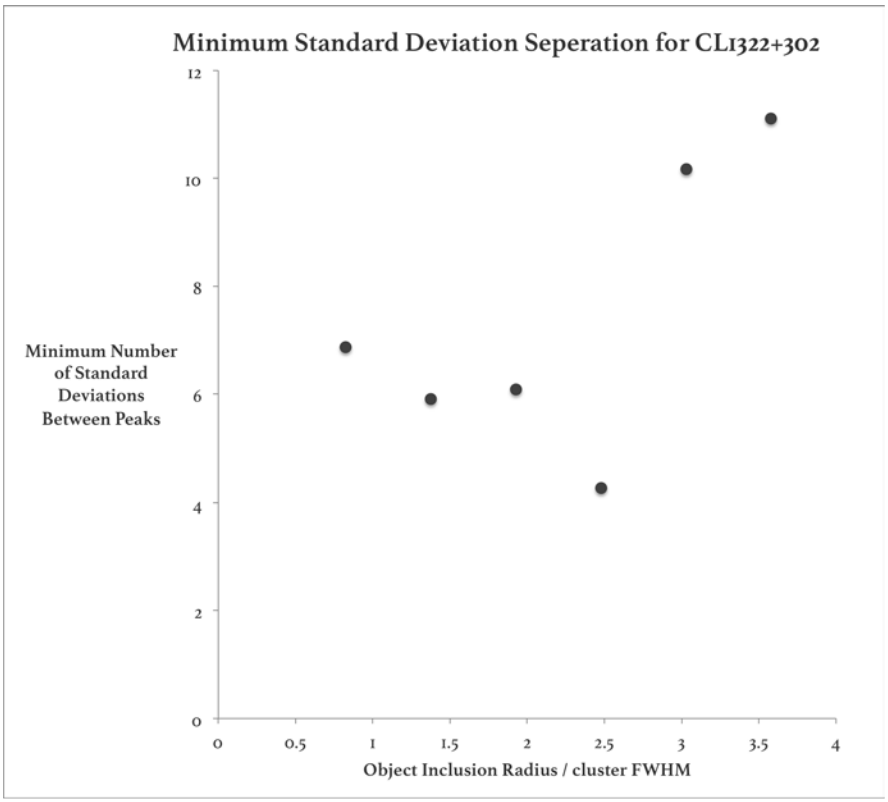

Figure 16: Minimum number of standard deviations between dark matter and number count density peaks for the cluster CL1322+302. The separation does not evolve monotonically as the inclusion radius is varied, which implies that there is inherent scatter in the peak location depending on what inclusion radius is chosen.

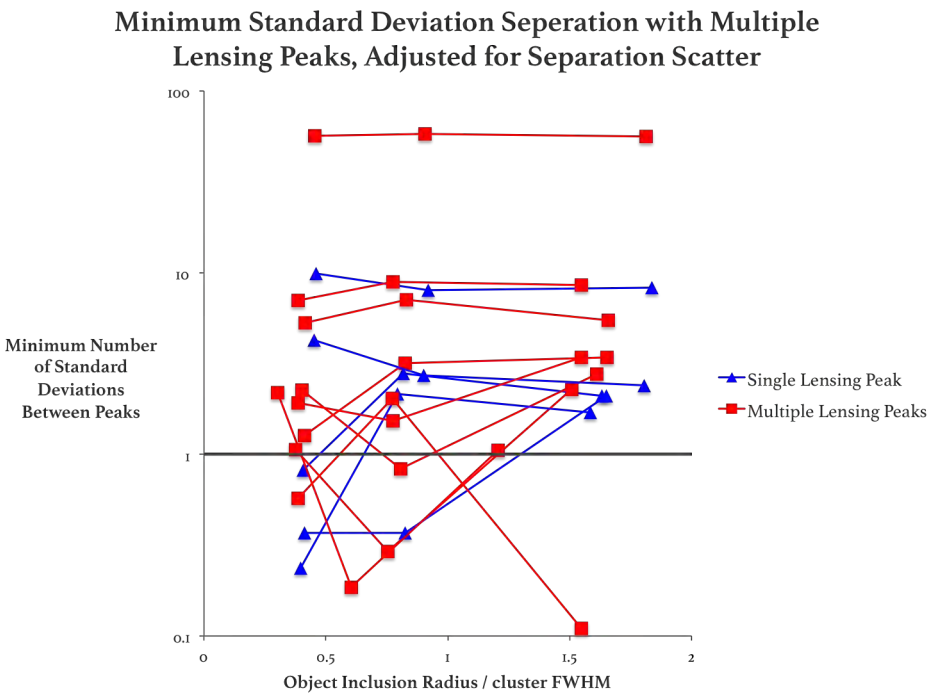

Figure 17: Identical to Figure 15, except adjusted for inherent scatter. The gray line demarcates a one standard deviation difference. There is still no clear difference between images with multiple lensing peaks and those with only one peak.

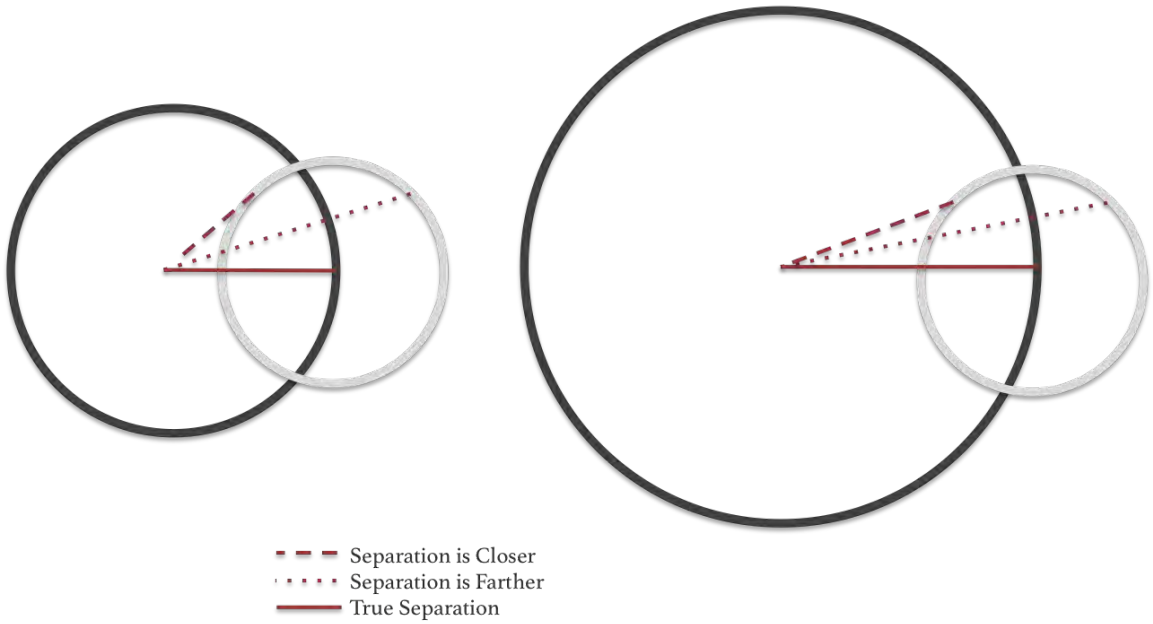

Figure 18: Left: the center of the darker circle represents one peak (for example, the lensing peak), and the center of the lighter circle represents the other peak (the number density peak). The darker circle represents all points the "true" separation distance away from the lensing peak. For a given uncertainty, the number density peak is shifted to a point on the lighter circle; as the figure demonstrates, there are fewer points on the lighter circle closer to the lensing center (that, is within the darker circle) than there are farther from the lensing center. On average, therefore, the separation is increased. Right: as the separation distance grows, the darker circle gets larger relative to the lighter one, and the separation distance becomes on average equal the true distance.

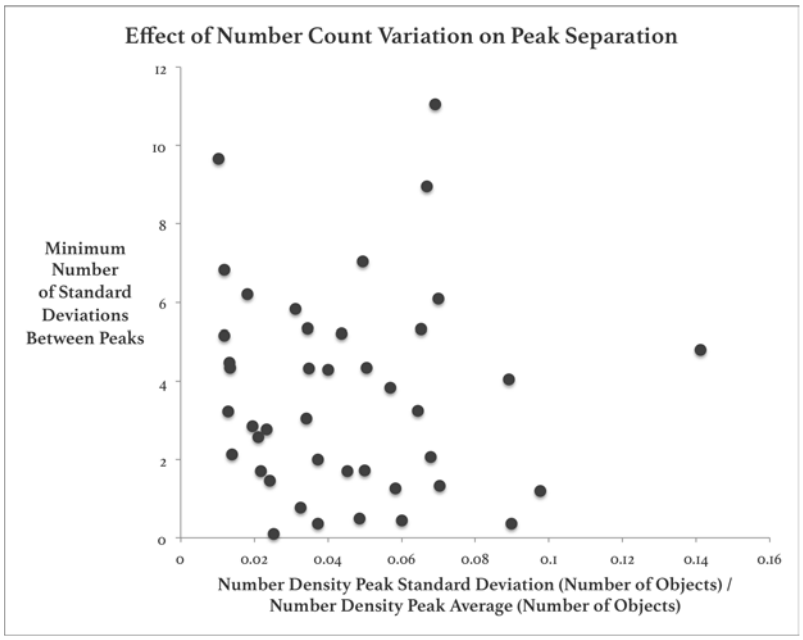

Figure 19: Peak separation plotted against the standard deviation in the number density peak value divided by the average value of the peak. There is no significant correlation.

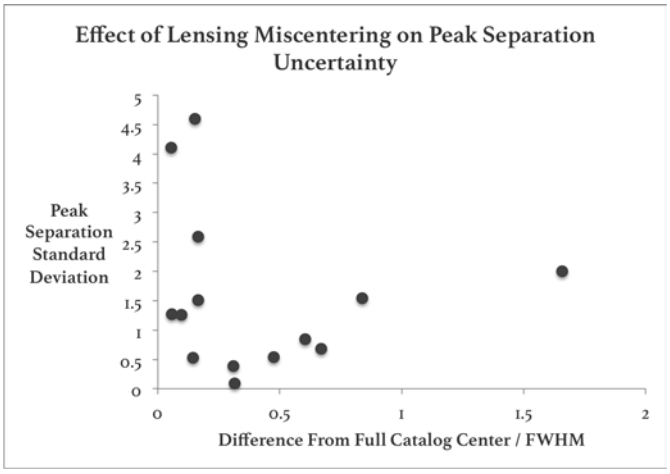

Figure 20: Peak separation plotted against the difference between the random catalog average lensing peak position and the full catalog lensing peak position, divided by the number count FWHM to normalize. There is no significant correlation.

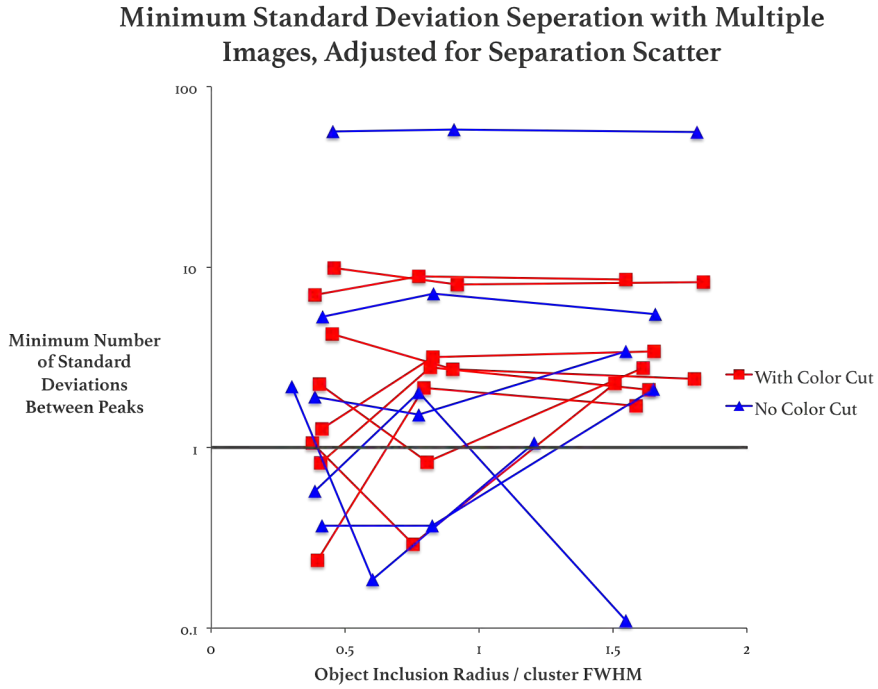

Figure 21: Adjusted minimum number of standard deviations between dark matter and number count density peaks for each cluster. The gray line demarcates a one standard deviation difference. There is no clear difference between clusters with color cuts and clusters without color cuts.

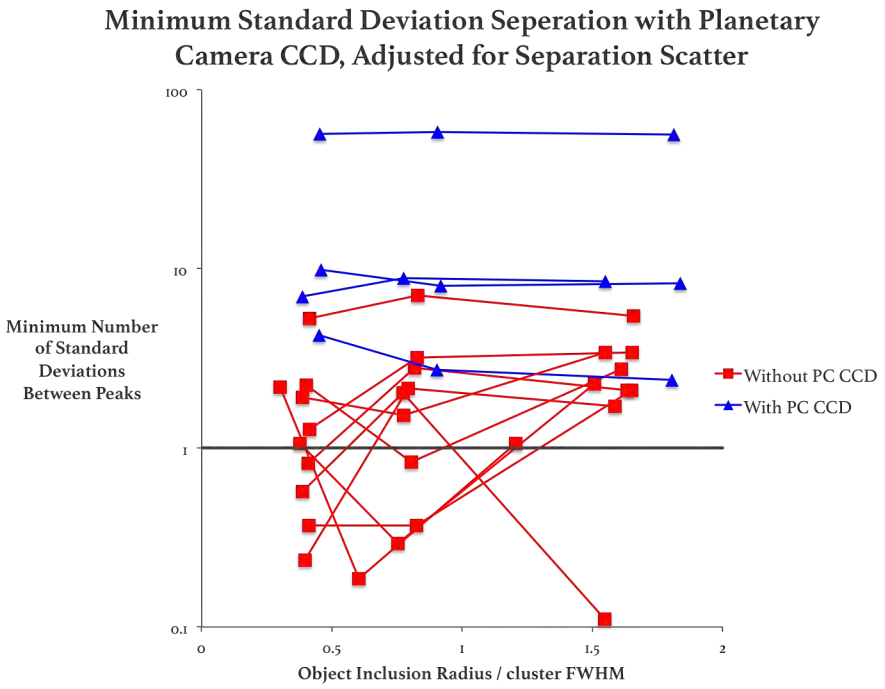

Figure 22: Adjusted minimum number of standard deviations between dark matter and number count density peaks for each cluster. The gray line demarcates a one standard deviation difference. There is indeed a difference between images with and without the PC, but it does not explain all of the excess separation.

4. CONCLUSION

The number density method provides a way of measuring the centroid of a galaxy cluster that is independent of redshift and can be carried out fairly quickly (once the procedure was developed, one cluster's analysis could be completed in a day or two). However, as Figure 15 shows, there are huge intrinsic variations in the separation depending on what inclusion radius is used, in clear contrast to the predictions made from the simulations of F14 shown in Figures 2 and 4. The variations do not seem to vary as a smooth function of the inclusion radius. While extra noise from the Planetary Camera CCD explains some of this variation, it does not explain all of it. Miscentering in the lensing or random variation in the number density peaks do not offer any correlation, and multiple explanations are still possible. Therefore, until this variability is better understood, this method does not allow a clear test of the SIDM hypothesis.

5. ACKNOWLEDGMENTS AND REFERENCES

I would like to thank Ian Dell'Antonio and Jacqueline McCleary for their help with this project. Part of this research was conducted using computational resources and services at the Brown University Center for Computation and Visualization.

1. Initial Evidence of Dark Matter. at <http://www.learner.org/courses/physics/unit/text.html?unit=10&secNum=2>

2. Ron Cowen & Davide Castelvecchi. European probe shoots down dark-matter claims. (2014). at <http://www.natur e.com/news/european-probe-shoots-down-dark-matter-claims-1.16462>

3. Boezio, M. et al. PAMELA and indirect dark matter searches. New J. Phys. 11, 105023 (2009).

4. NASA Finds Direct Proof of Dark Matter. at <http://c handra.harvard.edu/press/06_releases/press_082106.html?

5. Markevitch, M. et al. Direct Constraints on the Dark Matter Self-Interaction Cross Section from the Merging Galaxy Cluster 1E 065756. ApJ 606, 819 (2004).

6. Kahlhoefer, F., Schmidt-Hoberg, K., Frandsen, M. T. & Sarkar, S. Colliding clusters and dark matter self-interactions. MNRAS 437, 28652881 (2014).

7. Clowe, D. et al. A Direct Empirical Proof of the Existence of Dark Matter. ApJ 648, L109 (2006).

8. Surface Brightness Profiles. at <http://astronomy.swin.edu.au/cosmos/S/Surface+Brightness+Profiles>

9. Wide Field and Planetary Camera 2 Instrument Handbook Version 10.0. (2008). at <http://documents.stsci.edu/hst/wfpc2/documents/handbooks/cycle17/wfpc2_ihb.pdf>

10. Massey, R. et al. The behaviour of dark matter associated with four bright cluster galaxies in the 10 kpc core of Abell 3827. MNRAS 449, 33933406 (2015).

11. Ricker, P. M. & Sarazin, C. L. Off-axis cluster mergers: Effects of a strongly peaked dark matter profile. Astrophys.J. 561, 621644 (2001).

12. Dawson, W. A. et al. Discovery of a Dissociative Galaxy Cluster Merger with Large Physical Separation. ApJ 747, L42 (2012).

13. Lane, D. Testing Differences Between Means. at <http://onlinestatbook.com/2/tests_of_means/difference_means.html>